A hybrid microfluidic chip with electrowetting functionality using ultraviolet (UV)-curable polymer

Hao Gu,* Michel H. G. Duits and Frieder Mugele

Electrowetting (EW) is widely used in digital microfluidics for the manipulation of drops sandwiched between two parallel plates. In contrast, demonstrations of closed microfluidic channels enhanced with EW functionality are scarce. Here, we report a simple, low-cost method to construct such microchannels enclosed between two glass plates, each of which comprises electrodes and insulating layers. Our method uses soft imprint lithography with thiolene precursors to design the channel geometry. UV exposure is used to seal the chips permanently and a silanization treatment renders all inner channel surfaces hydrophobic. Compared to earlier polydimethylsiloxane-based designs, this method allows us to make microchannels with smaller dimensions (down to 10 microns), lower aspect ratios (down to height/length = 1/10), and symmetric electrodes both on the top and the bottom of the channel. We demonstrate the new capabilities with two examples: (i) EW-enhanced drop generation in a flow focusing geometry allows precise and continuous control on drop diameter in the range ≈ 1–15 microns while maintaining monodispersity; (ii) EW allows tuning of the excess water pressure needed to displace oil in a microchannel, leading to spontaneous imbibition at EW number $\eta > 0.89$.

1. Introduction

In the past decade, microfluidic systems have been increasingly applied to study, prepare and control two-phase fluids in various fields such as biology, medicine and food science.[1–4] Two-phase fluids in microfluidic chips also provide many possibilities in engineering, such as the controlled generation of emulsion drops serving as microreactors, controlled displacement of oil and water in microchannels, and logic operations with both bubbles and drops.[5–7] In all these cases, interfacial tensions and wetting phenomena play a prominent role in determining the flow behavior. This is due to the small length scales addressed in microfluidics, which introduce large surface-to-volume ratios, as well as strongly curved (e.g. water–oil) interfaces which in turn cause large Laplace pressures. These circumstances make it attractive to modulate the apparent interfacial tensions[8–11] rather than to apply (high) mechanical pressure for microfluidic actuation.

One of the promising methods for modulating the apparent solid–liquid interfacial tension is ElectroWetting (EW). This technique is attractive because of the simplicity of the device architecture, ease of electronic control and low energy consumption.[11–13] EW refers to an electrically induced reduction in contact angle of a conductive liquid on top of a dielectric-coated electrode in an insulating ambient medium. At present, most applications of EW are found in digital microfluidics in an open structure, where discrete operations on individual drops are carried out on the surface of a planar plate,[14,15] or in a sandwich geometry involving two parallel plates.[16–20] In both cases, EW allows for various manipulations with individual drops such as transporting, splitting and merging. Obviously, these open structures also have their limitations: in the first place, the drop manipulation rates and thereby the throughput of such EW devices is low compared to channel-based devices, because the maximum driving forces are limited by surface tension and contact angle saturation. Moreover, air, as an ambient medium, offers little protection for the drops against evaporation or contamination.

In previous studies, we extended the scope of EW to control two-phase flows in microchannels. To do so, we integrated insulator-covered electrodes into a flow-focusing device (FFD) leading to drop generation on demand and to electrical drop-size control, depending on the device geometry and operation mode.[21–23] For those prototype devices, microchannels were produced using soft lithography with thick slabs of PDMS and mechanically clamped onto EW surfaces consisting of ITO-glass slides covered by thin films of Teflon AF. These devices were easy to manufacture, but presented clear limitations: the softness and deformability of the PDMS allowed only for low clamping pressures, which limited both the possibilities for downscaling and the maximum flow rates. Moreover, the thickness of the PDMS slab precluded the integration of EW on the top surface, which makes the device asymmetric and reduces the maximum electrical forces by a factor of two. As with other PDMS based devices there are also restrictions regarding the choice of oil due to swelling. More sophisticated approaches not suffering from these drawbacks were recently presented by Heikenfeld et al.[24] and Kedzierski et al.[25] However, their devices were made using standard photolithography and wet chemical etching, which requires clean room facilities and advanced microfabrication skills.

Here we present a simple, rapid and inexpensive method to fabricate closed microchannels with integrated insulator-covered

Physics of Complex Fluids, Dept. of Science & Technology, IMPACT and MESA+ Institute, University of Twente, P. O. Box 217, 7500 AE Enschede, The Netherlands. E-mail: h.gu@tnw.utwente.nl; Fax: +31-(0)-53-489-1096; Tel: +31-(0)-53-489-4236

(EW) electrodes, which does not require cleanroom technology except for the initial fabrication of frequently reusable molds. Soft imprint lithography is applied to a liquid that is curable in ultraviolet (UV) light.[26] This approach has three advantages. First, the much higher stiffness of the final material (as compared to PDMS) allows to reduce the channel dimensions down to a few micrometers, even for rather small aspect ratios (height/ width < 1/10). Second, our new approach allows to manufacture symmetric devices with EW electrodes embedded into both the top and bottom surface of the microchannel. And third, the channel material is compatible with a broad selection of oils.

To demonstrate the capabilities of the new device, we fabricate two types of microfluidic devices with integrated EW functionality, namely (i) a FFD involving an orifice with much smaller dimensions than in our previous PDMS-based device and (ii) a straight microchannel, in which we can measure the imbibition pressure required to replace oil with water from a reservoir at controlled inlet pressure. (For practical reasons, the latter device also contains a T-junction.)

2. Experimental

Our chip designs are based on the UV curable material of Norland Optical Adhesive (NOA), which has recently found applications in various other microfluidic devices.[27–29] For our specific EW application, two additional issues had to be addressed: First, the bonding between NOA and Teflon AF coated surfaces had to be ensured. We found that a tight bonding could be achieved in spite of the known chemical inertness of Teflon AF. Second, NOA surfaces are prone to show poorly controllable wetting properties: both hydrophilic[28] and oleophilic[29] behaviors have been reported, and temporal changes in these properties cannot be excluded. Such variations pose a serious obstacle for controlling two-phase flows, which can be sensitive to small changes in wettability.[30,31] To overcome this problem, we applied a surface modification inside the assembled chip, which renders the NOA surfaces permanently hydrophobic, with contact angles that are comparable to those for Teflon AF.

2.1 Chip design and fabrication

To implement EW in microchannels, we started with commercial indium tin oxide (ITO)-coated glass (Prazisions Glas & Optik, Germany) as a substrate. Microchannels were fabricated using NOA 81 (Norland products). The general procedure for the soft imprint lithography part was adapted from Bartolo *et al.*[28] The specific fabrication steps are shown in Fig. 1. First a layer of Teflon AF 1600 (Dupont, USA) with a thickness of 3.2 µm was prepared by dip-coating [Fig. 1(a) and (f)].[32] To promote adhesion between NOA 81 and Teflon AF[33] surfaces, the Teflon AF was pretreated with oxygen plasma for 40 s at 100 W (PDC-32G, Harrick, USA) [Fig. 1(b)]. Subsequently, liquid NOA 81 was applied on Teflon AF-coated ITO glass, imprinted with the structured PDMS mold (RTV615, Bayer Silicones) and then cured by UV irradiation (UV crosslinker XL1500, Spectronics) for 38 s. [Fig. 1(c)]. After peeling the PDMS mold from the crosslinked NOA 81, microchannels were replicated on the bottom substrate [Fig. 1(d)]. A very thin layer of NOA 81 under the PDMS stamp remained incompletely cured because PDMS
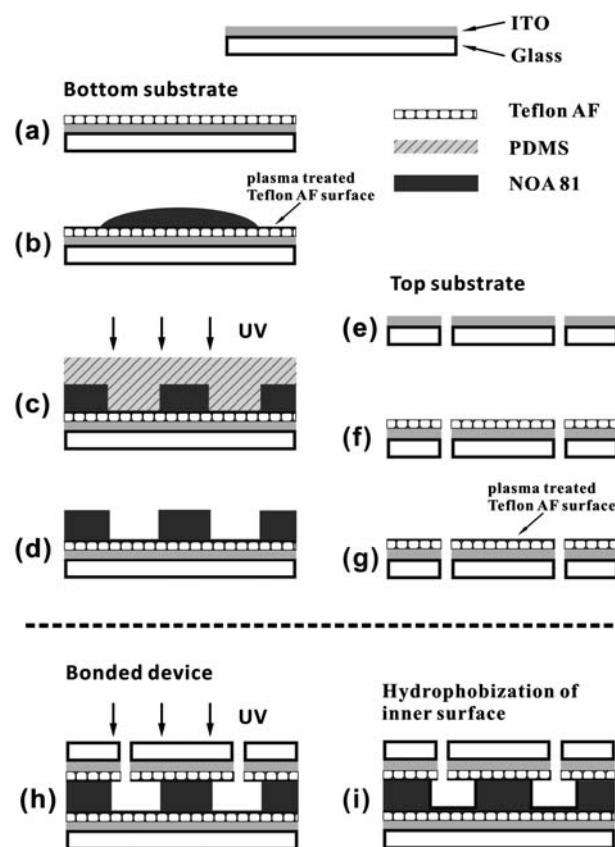

Fig. 1 Schematic of the fabrication process of our EW-based microchannel. (a)–(d) Imprinting the channel structure on a Teflon AF-coated bottom substrate; (e)–(g) drilling holes for inlet and outlet connections and then coating Teflon AF on the top substrate; (h) bonding the top and bottom substrates under UV exposure; (i) chemical modification of the inner channel.

facilitates the delivery of oxygen to the interface. This inhibits the free radical polymerization locally. With a properly controlled exposure time, complete curing of NOA in the boundary layer can be prevented.[34] The top surface was created from the same type of ITO–glass. After drilling holes for the inlet and outlet connections [Fig. 1(e)], the surface was coated with Teflon AF and an oxygen plasma treatment was applied to improve bonding with the bottom part [Fig. 1(g)]. Upon bringing the surfaces into contact, bonding was achieved by UV curing (for 180 s) of the previously mentioned thin layer of uncured NOA 81 on the bottom surface, leading to a permanently sealed microchannel [Fig. 1(h)]. The last step [Fig. 1(i)] was a surface modification to make the NOA 81 channel surfaces hydrophobic (see below).

2.2 Chemical surface modification

Except for the Teflon AF top surface, the inner walls of the microchannels are made of NOA 81. NOA 81 is hydrophilic (Young angle $\theta_Y < 90°$), which is not suitable for the application of EW, since a thin hydrophobic surface on the top of the dielectric layer and electrode is needed to optimize the EW effect in the standard EW configuration.[35] Hence a silanization treatment was applied, making the wettability of the NOA 81

comparable to that of the Teflon AF, *via* the deposition of a molecular monolayer. Based on the previous procedure used for silicon surfaces,[36–38] a 1.5% (v/v) solution of 1H,1H,2H,2H-perfluorodecyltrichlorosilane (FDTS) in isooctane was prepared under nitrogen, and pumped into the microchannel. After 15 min of incubation, excess FDTS was removed by flushing the channel with respectively isooctane and isopropanol, each for 20 min. The device was dried overnight at room temperature.

To examine the effects of the surface modification, we also coated a glass slide with NOA 81 and exposed it to UV irradiation and FDTS as for the channel and measured the contact angles of aqueous drops on them using an optical contact angle goniometer (OCA-15+, Data Physics, Germany) with built-in image analysis software.

2.3 Electrowetting experiments

Both the (EW enhanced) drop generation and imbibition experiments are performed using an aqueous dispersed phase (W) consisting of deionized water plus NaCl (conductivity: 5–7 mS/cm) and a continuous oil phase (O) of mineral oil (Sigma Aldrich M5904, viscosity: $\mu_O = 0.03$ Pa s) containing 5 wt% Span 80 as surfactant. The W/O interfacial tension (σ) was measured to be 5 mN/m with a plate method using a tensiometer (Kruss, Germany). In the drop generation experiments, the flow rates Q_w and Q_o were controlled using syringe pumps (Harvard PHD 2000, Harvard Apparatus). In the imbibition experiments, hydrostatic heads were used to control the pressures P_w and P_o.

EW was applied by connecting the top and bottom electrodes to an AC voltage source operating at a frequency of 10 kHz, and variable root-mean-square (rms) voltages U from 0 to 100 V_{rms}. (Similar results can also be achieved for frequencies down to ≈ 100 Hz.) The aqueous phase reservoir was connected to ground. The slope of the EW response of sessile drops on the flat surfaces prior to bonding yielded a capacitance of 5.4 $\mu F/m^2$, corresponding to an insulator thickness of 3.2 μm. The final chips containing the microchannels were mounted on the stage of an inverted microscope (TE 2000U, Nikon, Japan), equipped with a high-speed camera (Photron FASTCAM-Ultima 512, Japan). A 20×/air objective was used and images were captured at a frame rate of 2000 fps. ImageJ software (version 1.43n) was used to measure drop diameters.

3. Results and discussion

3.1 Characterization of surface hydrophobicity

To examine the effects of the surface modification, contact angles were measured for aqueous drops that were surrounded by either air or oil phase, while resting on flat substrates of NOA 81 and FDTS-coated NOA 81. The results summarized in Table 1 show that treatment with FDTS causes a contact angle (CA) increase from 70° to 112° in air, and from 96° to 156° in oil. For comparison: the respective CA values on Teflon AF are 110° and 156°. Clearly, the FDTS coating was successful, and an identical wettability was obtained for the Teflon AF and FDTS coated walls. Moreover, the long-term stability of the FDTS layer turned out to be very good, as evidenced by the minor variations in CA that were observed after 3 and 10 days of exposure to both air and oil phase (see Table 1).

Table 1 Contact angles for aqueous drops on NOA 81 surfaces with/without FDTS coating

Contact angle	NOA 81	FDTS-coated NOA 81		
		(right after treatment)	(3 days later)	(10 days later)
In air	70° ± 1°	112° ± 2°	110° ± 1°	111° ± 2°
In oil[a]	96° ± 2°	156° ± 2°	155° ± 2°	155° ± 2°

[a] Mineral oil with 5 wt % span 80.

Treatment with silanes is a well-known method for chemical modification of silicon and glass surfaces.[39,40] In many cases the silicon or glass surfaces are pre-treated by plasma or H_2O_2 to enhance the exposure of hydroxyl (*i.e.* silanol) groups. These –OH groups then react with the Si–Cl bonds of the fluorinated organosilane molecules to form Si–O–Si (*i.e.* siloxane) bonds. What happens chemically during the surface modification of UV-cured NOA 81 is less clear. In the uncured state, NOA 81 is a mixture containing trimethylol-propane tristhiol, isophorone diisocyanate ester, trimethylol-propane diallyl ether and benzophenone photo initiator. After the UV-induced crosslinking reaction, the –OH groups in trimethylolpropane diallyl ether are supposed to have remained.[41,42] A possible explanation for the good stability of the silanized NOA 81 surface could be that the allyl ether –OH groups reacted with Si–Cl bonds of the FDTS.

A clear difference between the silanization of NOA 81 as compared to glass or silicon is that NOA 81 does not require any pretreatment with oxygen plasma. On the contrary, we even find that such a pre-treatment has detrimental effects for the reliability of the resulting coating. Presumably, polymer chains break down and hydroxyl groups are eliminated from the NOA 81 surface during this treatment.

3.2 EW-controlled drop generation

For drop generation, a flow focusing geometry is used with an overall layout as in ref. 23. In the present version, the channel height H is 10 μm. The width of the orifice is $W = 20$ μm and the main channels have a width $W_m = 100$ μm. For drops that are formed *via* hydrodynamic breakup in a standard FFD, the size can be controlled *via* the flow rates of the inner and outer fluids. This produces drops of the order of the orifice size in the squeezing and in the dripping regime, and substantially smaller drops in the jetting and tip-streaming regimes. For devices comprising one side wall with EW functionaliy, it is possible to tune drop size and make smaller drops, as described in previous studies with a minimum orifice size of $W \times H = 50 \times 50$ μm.[23] In the current work, we demonstrate that even smaller drops can be generated in the "conical spray" regime, with more precise control, using as parameters the flow rates and applied voltages.

In the current experiments, the flow rate of the continuous oil phase, Q_o, was kept fixed at 60 $\mu l/h$, corresponding to a capillary number $Ca = \mu_o v/\sigma$ of 0.5, where v and μ_o are the average velocity and the viscosity of the oil phase, respectively. Drops were generated at three volumetric flow rates Q_w of the aqueous dispersed phase, corresponding to flow rate ratios of $\Phi = Q_w/Q_o$

= 1/6, 1/60 and 1/600. For each Φ, the AC voltage (U) was varied between 0 and 100 V_{rms}. The images shown in Fig. 2 clearly indicate that different regimes of drop generation are found for various combinations of U and Φ.

At the highest Φ (1/6), the generated drops are comparable to the dimensions of the orifice of the FFD [Fig. 2(a)–(f)]. The size distribution is monodisperse for voltages up to 40 V [(a)–(c)] but for $U > 60$ V a coexistence of drops with very different sizes is found in the downstream part [(d)–(f)]. High speed video recordings reveal that coalescence events prevent the production of monodisperse drops with $D < 10$ μm under these operating conditions.

The second column of Fig. 2 shows the results for $\Phi = 1/60$, *i.e.* a 10 times smaller Q_w. Again monodisperse drops are obtained for $U \leq 40$ V [(g)–(i)], but now the drops are clearly smaller due to the stronger shear forces that promote the neck formation and

breakup. For $U = 60$ V and higher voltages the drops are again polydisperse.

Upon reducing Q_w by another decade, *i.e.* to $\Phi = 1/600$, strings of uniform-sized drops are observed for $U \leq 40$ V [see (m)–(o)]. These drops are again substantially smaller than the ones created at a ten times higher Q_w. For $U > 60$ V, we now observe a conical spray, in which the drops spread out over a much wider range in the expanded downstream [(p)–(r)]. Interestingly, the tiny drops in this regime are rather monodisperse, which could be interesting for applications. This applies in particular to the case of $U = 100$ V, where also the generation rate of the drops is quite high (10^5 s^{-1}).

The resulting distribution of drop sizes is summarized in Fig. 3. It clearly indicates that at a constant AC frequency, the variation of Φ and U gives various ways for creating aqueous drops in the size range $\approx 1{\sim}15$ μm (diameter). At voltages up to 40 V, fairly
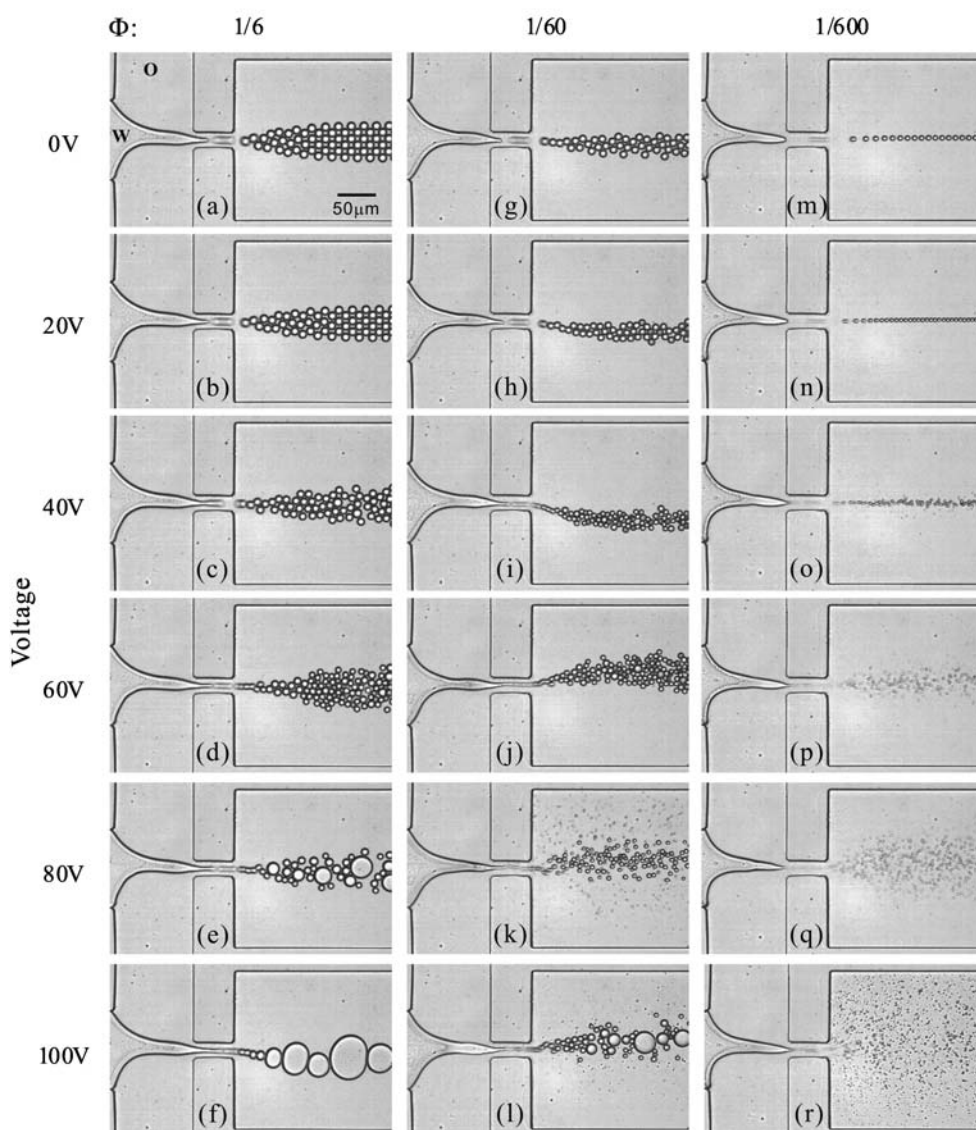

Fig. 2 Phase diagram for drop generation in a FFD, using three different flow rate ratios Φ of dispersed aqueous phase (W) and continuous oil phase (O). EW is used for additional control over drop generation. Here the voltage is applied to both top and bottom electrodes, while the aqueous reservoir is grounded. Q_o is 60 μl/h.
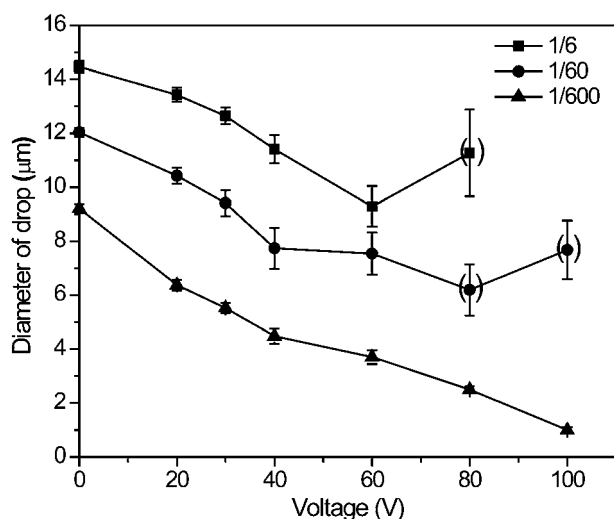
Fig. 3 Quantitative characterization of the drop size as a function of the EW voltage and the flow rate ratio Φ. Error bars indicate the standard deviation of the size distribution. Bracketed data points indicate cases where significant polydispersity was encountered; here only the primary drops were incorporated in the analysis.

monodisperse size distributions were found (polydispersity $\sigma_D \approx$ 1–4%) in all cases, while for $\Phi = 1/600$, σ_D was found to be $\leq 5\%$ even up to $U = 80$ V. At $U = 100$ V, the smallest drops appear to be smaller than 1 µm, but the size could not be more precisely measured due to limitations on the spatial resolution with the optical microscope. Knowing Q_w and (estimates of) D, also the drop generation rate can be calculated. Especially high rates (10^4–10^5 s^{-1}) are found in the conical spray regime with $D < 5$ µm.

What is the role of EW in the drop generation process? At low to moderate voltage (up to 40–60 V) the operation of the device is primarily controlled by hydrodynamic forces (pressure gradient, viscosity, interfacial tensions) and the general trends *e.g.* in drop size *vs.* Φ follow the observations from conventional (non-EW) microfluidic devices.[43] In this range, EW primarily changes the global shape of the oil–water interface by reducing the water CA on the channel walls.[44,45] Thereby EW provides different "boundary conditions" within which the hydrodynamic forces act. This leads to a rather efficient fine control over the drop sizes.

At voltages of order 60 V and higher, the role of EW becomes more dominant, leading amongst others to the onset of a completely different drop generation mechanism for small Φ, the conical spray formation. The wide lateral spreading of the small drops in the outlet region suggests that the drops in this conical spray regime carry electrical charge. This may be rationalized assuming that the drops are formed by a mechanism involving the electrical Maxwell stress as a primary driving force, similar to the generation of satellite drops during the instability of contact lines at high voltage in EW.[46–49]

Compared to the earlier PDMS-based devices with a single electrode on one channel wall, the new approach thus offers better and more continuous control over a wider range of drop sizes. Moreover, we note that, despite the small channel thickness and constriction the devices could be easily and stably operated at total flow rates of several thousand microliters per hour, which

is not possible with comparable PDMS devices due to elastic deformation. Apart from the well-known higher stiffness of NOA 81, this observation specifically highlights the strength of the bonding achieved between Teflon AF and NOA 81.

3.3 EW-driven imbibition of water in a 2-D channel

In the second application of the new design, we demonstrate directly the EW-induced variation of the pressure jump across W/O interfaces. To do so, we measure the critical hydrostatic pressure P_w^* on a water inlet, the "imbibition pressure", required to displace oil from an initially completely oil-filled channel. Here the oil pressure is controlled by another hydrostatic head at the oil inlet. For practical reasons, the microfluidic device also features an outlet channel, such that there is a continuous oil-stream [see Fig. 4(a)].

Similar to the experiments on the EW-controlled onset of drop generation described in ref. 21, the critical water pressure – here: for imbibition – is determined by the requirement that P_w must overcome the sum of the voltage-dependent Laplace pressure $\Delta P_L(\eta)$ of the W/O interface and local hydrostatic oil pressure $P_{o,loc}$

$$P_w^*(\eta) = \Delta P_L(\eta) + P_{o,loc} \qquad (1)$$

Fig. 5 shows the critical water pressure for a series of different oil pressures as a function of the applied voltage, which is expressed as the non-dimensional electrowetting number $\eta = CU^2/(2\sigma)$. (The electrowetting number expresses the electrical force per unit length pulling on the contact line in units of the W/O interfacial tension σ.[11]) Two trends are immediately observed: (i) P_w^* decreases linearly with η and (ii) $P_{o,loc}$ increases (linearly) with the oil inlet pressure P_o.

This voltage-dependence of P_w^* can be understood by considering the Laplace pressure of the W/O interface. It can be written as $\Delta P_L(\eta) \approx \sigma (1/R_W + 1/R_H)$, where R_W and R_H are the radii of curvature along the width and height of the channel, respectively. While R_W is constant, R_H varies with the contact angle $\theta = \theta(\eta)$ of the aqueous phase as $R_H = -H/(2cos\theta(\eta))$ (see inset of Fig. 5). (This expression is simpler than the
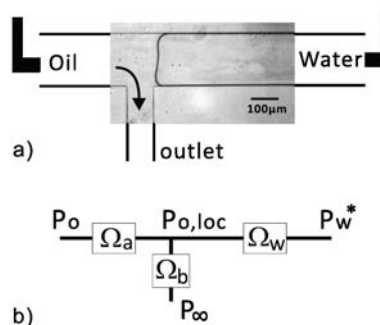

Fig. 4 (a) Magnified view of our setup for imbibition pressure measurements. Depending on the oil and water pressures at the W/O interface, either oil or water will flow through the channel. Use of EW electrodes allows favoring wetting of the hydrophobic walls in a quantitatively controllable manner. The width of main channel and side channel are 200 µm and 100 µm respectively. The channel height is 15 µm. (b) Hydraulic resistance circuit of the device.
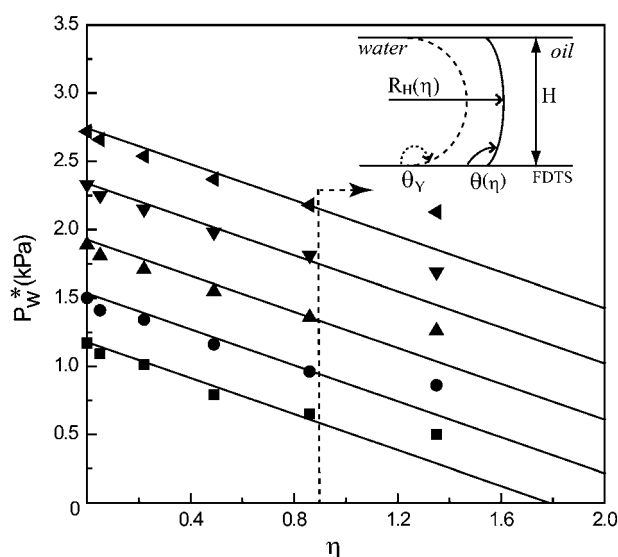
Fig. 5 Imbibition of the critical water pressure required for displacing the W/O interface, as a function of EW number (η) for different oil pressures (■: 1.47kPa, ●: 2.45kPa, ▲: 3.43kPa, ▼: 4.41kPa, ◀: 5.39kPa). The vertical dashed line indicates the critical EW number (*i.e.* voltage), beyond which ΔP_L is negative. Inset: cross-sectional sketch of the W/O interface inside the channel.

corresponding one in ref. 21 because the contact angle is the same on both surfaces and decreases in a symmetric way rather than only on one surface.) $\theta(\eta)$ is given by the EW equation $cos\theta(\eta) = cos\theta_Y + \eta$, as usual. This leads to the following expression for the voltage-dependent Laplace pressure:

$$\Delta P_L(\eta) = -\frac{2\sigma}{H}\eta - \frac{2\sigma}{H}\cos\theta_Y + \frac{2\sigma}{W} \qquad (2)$$

in agreement with the linear decrease shown in Fig. 5. The slope of the solid lines in Fig. 5 is thus given by $-2\sigma/H = -0.66$ kPa, as determined from independent measurements. The dashed vertical line indicates the critical EW number $\eta^* = 0.89$, at which ΔP_L of the W/O interface is zero. For all larger voltages the W/O interface has a negative mean curvature. (The data points for the highest voltage in Fig. 5 lie above this linear slope because contact angle saturation limits the contact angle reduction at high voltage (for a recent review on contact angle saturation, see ref. 50).

The relative vertical offset of the curves in Fig. 5 is due to the variation of $P_{o,loc}$ in eqn (1) with increasing oil inlet pressure. In analogy with Ohm's law, we find $P_{o,loc} = \Omega_b/(\Omega_a + \Omega_b)P_o = \lambda P_o$, where Ω_a and Ω_b the hydraulic resistances of the oil channel before and after the junction, respectively [see Fig. 4(b)]. Ω is related to the dimensions of the various channel segments by $\Omega \approx 12\mu_o L/WH^3$, where L is the length of the channel segment. (For the present geometry, we calculate $\lambda = 0.43$ in excellent agreement with the experimental result $\lambda = 0.41 \pm 0.01$ obtained from the vertical offset of the solid lines in Fig. 5.)

These results illustrate several advantages compared to our earlier approach using PDMS-based devices: (i) due to the enhanced stiffness of NOA 81 compared to PDMS, it is possible to produce not only overall smaller microchannels but also microchannels with a very small aspect ratio. In this case, the

influence of the side walls on the mean curvature of the W/O interface is reduced, leading to a wider tunability of the pressure. Moreover, the flow geometry is almost two-dimensional. (ii) For the PDMS-devices, the contact angle on the top surface remains constant at a rather large value of $\approx 160°$. As a consequence, ΔP_L is always positive, even at the highest accessible values of η. With the present symmetric device, this limitation can be overcome and truly negative mean curvatures of the W/O interface can be achieved. As a consequence, these symmetric devices allow sucking water into an initially oil-filled microchannel from a larger reservoir at zero pressure. This may be useful for the loading of microfluidic chips, which usually requires sealing micropipettes to inject liquid at an overpressure.

4.   Conclusions

In summary, we developed a simple and inexpensive fabrication technique for microfluidic chips, which combine the functionalities of channel flow and EW. The imprinting lithography based on NOA 81 offers the opportunity to build devices with micron size features. Reliable hydrophobization of the NOA 81 surface is achieved using a silanization treatment. The new chip design allows for a more precise and continuous control over the formation of monodisperse small drops with diameters from 1 to 15 μm in flow focusing devices. Moreover, it allows for controlling the pressure (and thus the actuation force) in the aqueous phase over a much wider range (including negative Laplace pressures) than asymmetric devices. Amongst other aspects, this enables spontaneous filling (imbibition) of water into microchannels from macroscopic reservoirs at zero pressure.

References

1 H. A. Stone, A. D. Stroock and A. Ajdari, *Annu. Rev. Fluid Mech.*, 2004, **36**, 381–411.
2 H. Song, D. L. Chen and R. F. Ismagilov, *Angew. Chem., Int. Ed.*, 2006, **45**, 7336–7356.
3 G. M. Whitesides, *Nature*, 2006, **442**, 368–373.
4 R. B. Fair, A. Khlystov, T. D. Tailor, V. Ivanov, R. D. Evans, P. B. Griffin, V. Srinivasan, V. K. Pamula, M. G. Pollack and J. Zhou, *IEEE Des. Test Comput.*, 2007, **24**, 10–24.
5 M. J. Fuerstman, P. Garstecki and G. M. Whitesides, *Science*, 2007, **315**, 828–832.
6 M. Prakash and N. Gershenfeld, *Science*, 2007, **315**, 832–835.
7 M. Schindler and A. Ajdari, *Phys. Rev. Lett.*, 2008, **100**, 044501.
8 T. S. Sammarco and M. A. Burns, *AIChE J.*, 1999, **45**, 350–366.
9 A. A. Darhuber and S. M. Troian, *Annu. Rev. Fluid Mech.*, 2005, **37**, 425–455.
10 R. B. Fair, *Microfluid. Nanofluid.*, 2007, **3**, 245–281.
11 F. Mugele and J. C. Baret, *J. Phys.: Condens. Matter*, 2005, **17**, R705–R774.
12 C. Quilliet and B. Berge, *Curr. Opin. Colloid Interface Sci.*, 2001, **6**, 34–39.

13 M. G. Pollack, A. D. Shenderov and R. B. Fair, *Lab Chip*, 2002, **2**, 96–101.

14 C. G. Cooney, C. Y. Chen, M. R. Emerling, A. Nadim and J. D. Sterling, *Microfluid. Nanofluid.*, 2006, **2**, 435–446.

15 S. Berry, J. Kedzierski and B. Abedian, *J. Colloid Interface Sci.*, 2006, **303**, 517–524.

16 J. Lee and C. J. Kim, *J. Microelectromech. Syst.*, 2000, **9**, 171–180.

17 S. K. Fan, P. W. Huang, T. T. Wang and Y. H. Peng, *Lab Chip*, 2008, **8**, 1325–1331.

18 J. Gong and C. J. Kim, *Lab Chip*, 2008, **8**, 898–906.

19 M. J. Jebrail and A. R. Wheeler, *Anal. Chem.*, 2009, **81**, 330–335.

20 D. Brassard, L. Malic, F. Normandin, M. Tabrizian and T. Veres, *Lab Chip*, 2008, **8**, 1342–1349.

21 F. Malloggi, S. A. Vanapalli, H. Gu, D. van den Ende and F. Mugele, *J. Phys.: Condens. Matter*, 2007, **19**, 462101.

22 F. Malloggi, H. Gu, A. G. Banpurkar, S. A. Vanapalli and F. Mugele, *Eur. Phys. J. E*, 2008, **26**, 91–96.

23 H. Gu, F. Malloggi, S. A. Vanapalli and F. Mugele, *Appl. Phys. Lett.*, 2008, **93**, 183507.

24 J. Heikenfeld, K. Zhou, E. Kreit, B. Raj, S. Yang, B. Sun, A. Milarcik, L. Clapp and R. Schwartz, *Nat. Photonics*, 2009, **3**, 292–296.

25 J. Kedzierski, S. Berry and B. Abedian, *J. Microelectromech. Syst.*, 2009, **18**, 845–851.

26 Y. N. Xia and G. M. Whitesides, *Annu. Rev. Mater. Sci.*, 1998, **28**, 153–184.

27 Z. T. Cygan, J. T. Cabral, K. L. Beers and E. J. Amis, *Langmuir*, 2005, **21**, 3629–3634.

28 D. Bartolo, G. Degre, P. Nghe and V. Studer, *Lab Chip*, 2008, **8**, 274–279.

29 L. H. Hung, R. Lin and A. P. Lee, *Lab Chip*, 2008, **8**, 983–987.

30 B. Zhao, J. S. Moore and D. J. Beebe, *Science*, 2001, **291**, 1023–1026.

31 W. Li, Z. H. Nie, H. Zhang, C. Paquet, M. Seo, P. Garstecki and E. Kumacheva, *Langmuir*, 2007, **23**, 8010–8014.

32 E. Seyrat and R. A. Hayes, *J. Appl. Phys.*, 2001, **90**, 1383–1386.

33 J. Scheirs, *Modern Fluoropolymer*, John Wiley & Sons, Ltd., New York, 1997.

34 J. P. Rolland, E. C. Hagberg, G. M. Denison, K. R. Carter and J. M. De Simone, *Angew. Chem., Int. Ed.*, 2004, **43**, 5796–5799.

35 A. Quinn, R. Sedev and J. Ralston, *J. Phys. Chem. B*, 2005, **109**, 6268–6275.

36 K. Handique, D. T. Burke, C. H. Mastrangelo and M. A. Burns, *Anal. Chem.*, 2000, **72**, 4100–4109.

37 B. J. Adzima and S. S. Velankar, *J. Micromech. Microeng.*, 2006, **16**, 1504–1510.

38 L. L. Shui, A. van den Berg and J. C. T. Eijkel, *Lab Chip*, 2009, **9**, 795–801.

39 J. Sagiv, *J. Am. Chem. Soc.*, 1980, **102**, 92–98.

40 A. del Campo and I. J. Bruce, *Top. Curr. Chem.*, 2005, **260**, 77–111.

41 B. S. Chiou, R. J. English and S. A. Khan, *Macromolecules*, 1996, **29**, 5368–5374.

42 X. Q. Gong, W. J. Wen and P. Sheng, *Langmuir*, 2009, **25**, 7072–7077.

43 P. Garstecki, H. A. Stone and G. M. Whitesides, *Phys. Rev. Lett.*, 2005, **94**, 164501.

44 J. Buehrle, S. Herminghaus and F. Mugele, *Phys. Rev. Lett.*, 2003, **91**, 086101.

45 NOTE: If the channel thickness H approaches the insulator thickness d, additional aspects may become relevant: Since the electrical stresses in EW are distributed over a region of order d, the additional distortions of the oil–water interface arise (rather than a simple reduction of the contact angle) that will affect the drop generation. See ref. 44. For the current device with d = 3.2 μm and H = 10 μm, it is currently not clear to what extent these effects already matter.

46 M. Vallet, M. Vallade and B. Berge, *Eur. Phys. J. B*, 1999, **11**, 583–591.

47 F. Mugele and S. Herminghaus, *Appl. Phys. Lett.*, 2002, **81**, 2303–2305.

48 NOTE: Since the capacitance between the small drops to be formed and the electrodes on the substrate is small, it is natural that the drops aquire some charges during the breakup process that they do not dischardge. see ref. 49.

49 J. C. Baret and F. Mugele, *Phys. Rev. Lett.*, 2006, **96**, 016106.

50 F. Mugele, *Soft Matter*, 2009, **5**, 3377–3384.